Chapter 5
Nanomaterials for Effective Control of Algal Blooms in Water

Rong Cheng, Liang-jie Shen, Shao-yu Xiang, Dan-yang Dai, and Xiang Zheng

Abstract Algal blooms resulted from eutrophication has increasingly occurred worldwide and poses serious threats to water environment, tourism and aquatic ecosystems. In addition, the toxins released by living or dead algae are harmful to aquatic animals or even the human body. Hence, the effective control of algal blooms becomes an urgent front-burner problem. Nanotechnology, the emerging means, has produced great repercussions in recent decades because of its unique physical and chemical properties such as small-size effect, quantum-size effect and so forth. Considering the source controlling, short-term strategy and health risk, the removal of nutrient, algae or algae toxins from the water using nanotechnology is reviewed in this text. Firstly, the removal performance and mechanisms of phosphorus by nanomaterials are summarized from the view of source controlling. And the major point is that the nanoparticles present extremely high capacity (5–200 mg $P \cdot g^{-1}$) and specific affinity to phosphorus. Then, the effect on algae removal by nanomaterials is analyzed from the short-term strategies. And the removal efficiency is increased with the dose of nanoparticles and the algae are removed and destructed through the photocatalytic oxidation. Furthermore, mechanisms of photocatalytic removal of algae are discussed. And the algae toxins (e.g. microcystin-LR) can be adsorbed or degraded by nanoparticles (e.g. magnetic materials or nano-photocatalyst). Finally, the current challenges are outlined and future directions to achieve efficient and economic control of algal blooms are discussed.

Keywords Algal bloom · Nanomaterials · Eutrophication · Phosphorus · Algal toxins · Microcystins

R. Cheng (✉) · L.-j. Shen · S.-y. Xiang · D.-y. Dai · X. Zheng (✉)
School of Environment and Natural Resources, Renmin University of China, Beijing, China
e-mail: chengrong@ruc.edu.cn; shenliangjie@ruc.edu.cn; xiangshaoyu@ruc.edu.cn; daidanyang@ruc.edu.cn

N. Dasgupta et al. (eds.), *Environmental Nanotechnology Volume 5*,
Environmental Chemistry for a Sustainable World 37,
https://doi.org/10.1007/978-3-030-73010-9_5

5.1 Introduction

Algae bloom is mainly caused by the eutrophication, which is the phenomenon of excessive phytoplankton production in rivers, lakes and reservoirs, resulted from increases in levels of nutrients (phosphorus and nitrogen compounds) (Zamparas and Zacharias 2014). The organic matters produced by algae affect the color, taste and odor of drinking water and even a number of cyanobacterial species excrete toxic metabolites (Microcystin-LR, Microcystin-RR and so forth), which can cause worse health problems (O'Neil et al. 2012).

Phosphate is one of the important nutrients which are indispensable for all creatures on the earth. Excessive presence of phosphorous in water bodies, however, is one of the major causes to eutrophication, which leads to the outbreaks of algae bloom, diminishes dissolved oxygen, lowers water quality, and reduces biodiversity in aquatic ecosystems (Hartmann et al. 2010; Zhang et al. 2009; Yang et al. 2013; Saha et al. 2009). As shown in Fig. 5.1, the problem of eutrophication all over the world is abominable and urgent to be solved (Liu et al. 2016).

So the corresponding limiting concentration of phosphate in surface water and products containing phosphorus is provided in almost all countries, such as 0.010 ~ 0.100 mg·L^{-1} for river and 0.005 ~ 0.050 mg·L^{-1} for lakes and reservoirs in Australian, 0.02 ~ 0.40 mg·L^{-1} for lakes and reservoirs in China, less than 0.3 g per standard dose for cleaning agent of kitchen utensils and less than 0.5 g per standard dose for washing powder in European Union, less than 50 μg·L^{-1} for United States Environmental Protection Agency (USEPA) and so forth. The high concentration of phosphate (e.g. PO_4^{3-}, HPO_4^{2-} and $H_2PO_4^-$) in water is attributed to various sources,

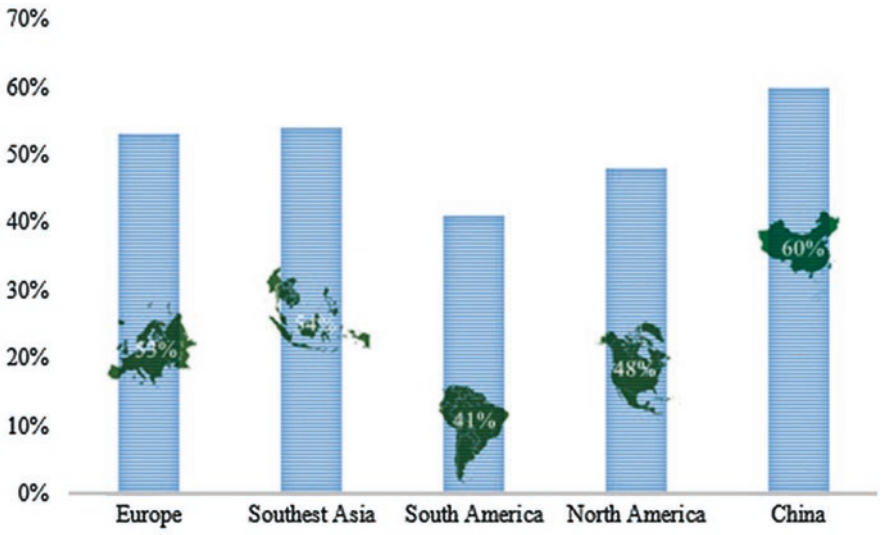

Fig. 5.1 The proportion of eutrophic water bodies in various regions

including agricultural pollution, municipal or industrial wastewater disposal and natural solubilization of rocks (Zhou et al. 2001; Pieterse et al. 2003). Therefore, it is of vital importance to reduce and control the level of phosphorous in the industrial, urban, and agricultural wastewater prior to its discharge into environment, and phosphate removal from water has attracted considerable research interest in the last few decades (Kasp et al. 2005).

In addition, the water is in a long-term anoxic state caused by the algae bloom, which leads to the death of a large number of water organisms and the stink of water quality, and affects the healthy operation of the whole aquatic ecosystem (Wolf et al. 2017). To make matters worse, such problems led to aquaculture bankruptcy and deficits. And it is worrisome that algal toxins produced from algae blooms are highly toxic to both of the aquatic organisms and humans with incalculable consequences (Meneely and Elliott 2013; Wiegand and Pflugmacher 2005).

In the face of frequent algae bloom, and the consequent losses, how to solve the problems becomes urgent. On the whole, the most important and primary problem is the excess nutrient in water, especially phosphorus (Chouyyok et al. 2010). What we need to consider next is the removal of a large amount of algae in the water (Barrado-Moreno et al. 2017). Then, the removal of algae toxins released into the body of water after algae bloom is also a challenging task (Meneely and Elliott 2013). Considering the source controlling, short-term strategy and health risk, the removal of phosphate, algae or algae toxins from the water using nanotechnology is reviewed in this text.

5.2 Removal of Phosphate by Nano-materials in Water

Traditionally, several methods, including chemical precipitation, biological treatment, ion exchange and adsorption, have been investigated to remove phosphorous from aqueous solution. In particular, the adsorption-based process is considered as one of the promising routes, due to ineffectiveness of toxic substance, and recyclability of adsorbents (Yu and Chen 2015). In the last decades, a lot of efforts have been devoted to the exploitation of various adsorbents for fast removal of phosphate in water bodies including natural red mud, ash, iron oxide and metal-based materials (Haghseresht et al. 2009; Lu et al. 2009; Zeng et al. 2004). Various transitional metallic oxides are proved to be efficient adsorbents for phosphate retentions by strong inner-sphere complexation of metallic oxides such as zirconium oxides and iron oxides. The development of metal (e.g. Al, Fe, Ti, and so on.) doped or modified materials as adsorbents for enhanced phosphate removal has become an increasing area of research, thanks to the specific adsorption between metal active sites and phosphate in solution (Delaney et al. 2011; Li et al. 2013). Compared to other metals, lanthanum-based adsorbents show a number of promising advantages in phosphate removal, including superior adsorption capacity, wide operating pH range and high removal rate in a low phosphate concentration. It's reported that lanthanum oxides are confirmed to possess ultra-high activity for phosphate sequestration,

approximately ten times greater than that of famous aluminum oxides powder (Xie et al. 2015; Lürling et al. 2014).

In the 1970s, phosphate precipitation by lanthanum was found to be more effective over a wider pH range (4.5 ~ 8.5) than either Fe^{3+} or aluminium salts (Melnyk 1974). It is known that rhabdophane ($LaPO_4$) is insoluble in aqueous medium, it is thus imaginable that lanthanum or lanthanum oxide based materials should facilitate the adsorption or removal of phosphate due to the formation of $LaPO_4$ (Kuroki et al. 2014). Recently, there has been tremendous interest, concentrating on the nanosized lanthanum-based adsorbents and their potential in different practical applications (Huang et al. 2014a, b, 2015a, b; Zong et al. 2017; Lai et al. 2016).

Some review papers have been devoted to the removal of phosphate in terms of mesoporous materials, lanthanum modified bentonite and so on (Huang et al. 2017; Copetti et al. 2016). However, there have been few reviews on the development of nanosized lanthanum-based adsorbents especially targeting at phosphate removal. In this work, the synthesis and performance of various nanosized La-based adsorbents were summarized, as well as the influence factors (pH, ionic strength, and coexisting anion).

According to the properties and types of carriers, the nanosized La-based adsorbents that have been used for phosphate control are classified into five categories: La-clay mineral adsorbents, La-metallic compounds, La-organics adsorbents, La-silica adsorbents and La-others. To provide a global overview of the state of the art, there are nearly two hundred scientific publications dealing with the removal of phosphate by La-based adsorbents. Figure 5.2 shows the numbers of publications on nanosized La–based adsorbents for phosphate removal in *Web of Science*.

As shown in the Fig. 5.2a, the research on nanosized La-based adsorbents for phosphate removal is generally on the rise, especially in recent years. In Fig. 5.2b, the main status is occupied by La-clay minerals accounting for 48.2%. It's understandable that clay minerals are an important class of adsorbents that comprise of a broad range of porous crystalline solids and based essentially on tetrahedral networks which encompass channels and cavities. For La-organic adsorbents like La-chitosan, Chitosan (poly-β-(1 → 4)-2-amino-2-deoxy-D-glucose) is a natural polysaccharide produced by the N-deacetylation of chitin and its high amino content on the polymer matrix provides selectivity to the adsorption process.

5.2.1 Removal of Phosphate by Nanosized La-Based Adsorbents

5.2.1.1 Preparation and Mechanism of Nanosized La-Based Adsorbents

The adsorbent has high specific surface area and abundant pores, such as 600 ~ 900 $m^2 \cdot g^{-1}$ for bentonite, 400 ~ 800 $m^2 \cdot g^{-1}$ for zeolite. The large surface area leads to great surface energy, together with its layered structure and the type and distribution of elements in the structure, which determine its strong adsorption

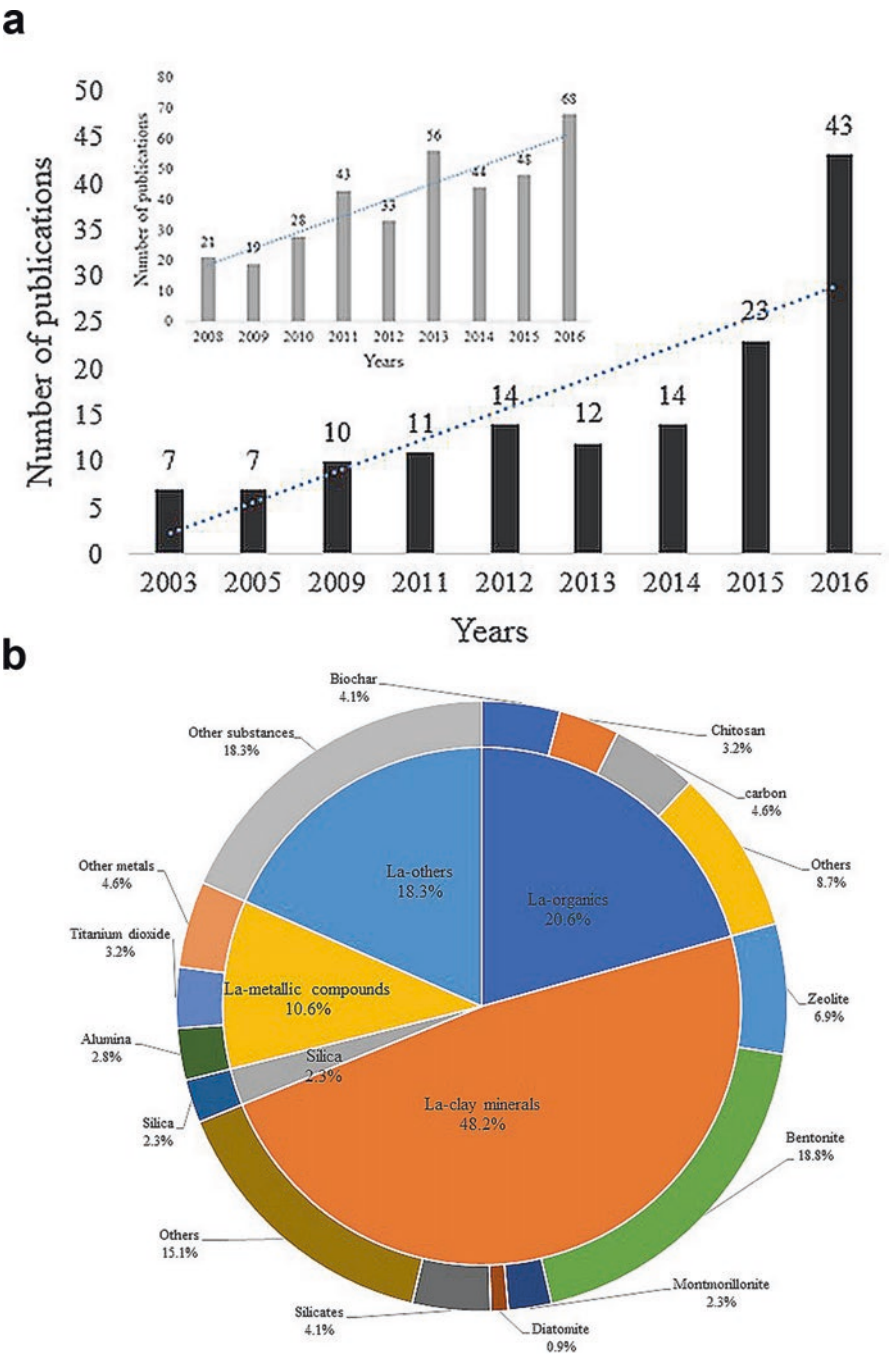

Fig. 5.2 (**a**) Numbers of publications on nanosized La-based adsorbents per year (numbers of publications on adsorbents were inseted); (**b**) Percentages of different types of nanosized La-based adsorbents

capacity. However, single adsorbent fails to achieve the specific selectivity and its structure is not optimal. So further modification is required, and La modification has gradually attracted the interest of scholars in recent years. And adsorbents with good property generally serve as the matrix for immobilizing the nanosized La compounds.

Preparation of Nanosized La-Based Adsorbents

Nanosized La-based adsorbents have been used for phosphate removal for approximately 40 years. Various types of adsorbents have been synthesized and studied for the recovery of water.

1. **La-clay mineral adsorbents**

La-clay mineral adsorbents are one of the most widely used materials and successfully applied for the phosphate removal in both water and wastewater because of the easy access, low cost and excellent adsorption of clay minerals (Epe et al. 2017). Typically, impregnation is used most for preparing the La-clay mineral adsorbents, by which the lanthanum ions (0.112 nm for ionic radius of La^{3+}) would enter the pores and surface of clay minerals due to the mode of ion exchange process and free diffusion (Kuroki et al. 2014; Haghseresht et al. 2009). Then, the sample was dried at relatively higher temperatures (e.g. 383 K) to form lanthanum oxides.

The preparation of La-clay mineral with impregnation is relatively simple, but the selection of appropriate carrier should be paid more attention. As shown in Table 5.2, the adsorption capacity of different types of clay minerals is not uniform after loading with lanthanum, and the specific surface area (S_{BET}) and pore size distribution of different clay minerals are different (Ning et al. 2008; Li et al. 2009).

2. **La-metallic compounds**

Normally, La-metallic compounds are synthetized with co-precipitation method. Lanthanum is co-precipitated with other metals, such as Fe or Al. The corresponding metal salts were selected and co-precipitation was achieved under suitable reaction conditions.

3. **La-organics adsorbents**

In most cases, the acid treatment or alkali treatment is first subjected to the organic adsorbents for removing the remaining impurities and dredging channels. It is beneficial to the diffusion of lanthanum anions or particles. Lanthanum was modified or doped into the corresponding adsorbents by oxide-reduction reaction.

Generally, the adsorbent, supporting the lanthanum, was first gained and then put into the solution containing lanthanum ions ($La(NO)_3 \bullet 6H_2O$ as the precursor) for impregnating several hours. Then, the reducing agent (ammonia, sodium hydroxide, ammonium hydrogen carbonate) is added into mixed solution to generate the lanthanum oxide or hydrated lanthanum compound. The equation is as follows:

$$La^{3+} + OH^- \rightarrow La(OH)_3 \downarrow \rightarrow La_2O_3 \downarrow + H_2O \tag{5.1}$$

Lanthanum hydroxide loaded on adsorbent must be treated at high temperature to transform to lanthanum oxide as shown in Table 5.1 and Fig. 5.3.

5.2.1.2 Mechanism of Phosphorus Adsorption

There is no doubt that the whole process of phosphate removal is dominated by adsorbents. From Table 5.2, we can see that adsorbents are almost found to better match with the pseudo-second-order model ($R^2 > 0.99$) than the pseudo-first-order model, suggesting the adsorption process be chemisorption. It means that the phosphate ions in the solution undergo electron transfer or exchange with the lanthanum atoms or molecules modified in surface or interior of adsorbents. Meanwhile, The Langmuir model is more suitable for nanosized La-based adsorbents, which means that observed adsorption onto nanosized La-based adsorbents is caused by the monolayer coverage.

The selective adsorption of the adsorbent is based on the property of adsorbent matrix and indirectly obtained by modification. Lanthanum is used to corresponding adsorbent for gaining better adsorption capacity of phosphate. The following reaction would be the mechanism responsible for the adsorption of phosphate by lanthanum (Xie et al. 2015; Huang et al. 2014a, b):

$$La - OH + HPO_4^{2-} \leftrightarrow La - HPO_4^- + OH^- \tag{5.2}$$

$$La - OH + H_2PO_4^- \leftrightarrow La - H_2PO_4 + OH^- \tag{5.3}$$

$$La = (OH)_2 + HPO_4^{2-} \leftrightarrow La = HPO_4 + 2OH^- \tag{5.4}$$

$$La \equiv (OH)_3 + PO_4^{3-} \leftrightarrow La \equiv PO_4 + 3OH^- \tag{5.5}$$

The mechanism might involve ion complexation during subsequent adsorption of phosphorus on lanthanum. It is showed that the ligand-exchange process at high pH levels on lanthanum (hydr) oxide surfaces. The diagram is shown in Fig. 5.3.

Table 5.2 presented the most representative examples of the nanosized La-based adsorbents employed for the removal of phosphate from eutrophic water.

From Table 5.2, under the same conditions, with the increase of lanthanum loading, the removal rate was obviously improved. It's obvious that the greater amount of molar ratio of adsorbed P versus La (P/La), the higher the effective utilization of la active sites simultaneously. Furthermore, the adsorption of phosphate on most nano-materials fits the pseudo-second-order model, indicating that the phosphate adsorption process is likely governed by chemisorption. However, there are still some adsorbents in line with the pseudo-first-order kinetics. And the adsorption process was well described by the intraparticle diffusion model.

Table 5.1 Comparison of preparation methods of materials

Method		Experiment process	References
calcination	/	Mixture is stirred at 60 °C for 24 h and was calcined at 550 °C for 5 h	Huang et al. (2013)
Oxide-reduction	Calcination	Reacting $La(NO)_3 \bullet 6H_2O$ with NH_4HCO_3; dried at 110 °C followed by calcination at 750 °C in a vacuum tube furnace for 6 h	Chen et al. (2015a, b)
Electrospinning	/	Polyacrylonitrile and nano-La_2O_3 are dissolved in DMF (80 °C for 2 h); then electrospinning process (15 kV, 20 cm, 1.0 mL·h^{-1})	He et al. (2016)

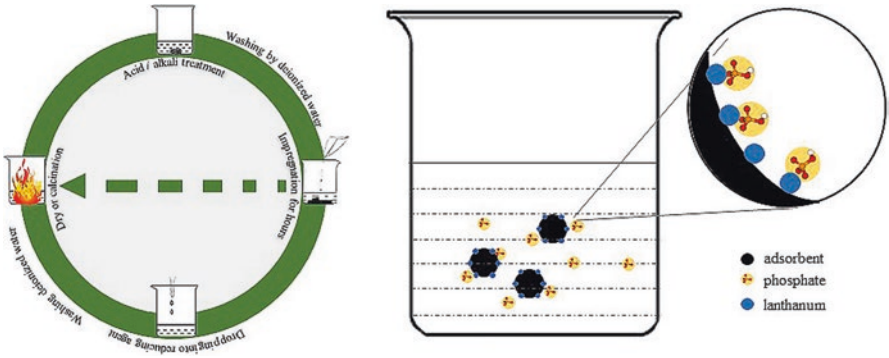

Fig. 5.3 Mechanism of material preparation and sketch map of phosphorus adsorption

5.2.2 Influence Factors of Phosphate Removal by Nanosized La-Based Adsorbents

Based on the interaction between nanosized La-based adsorbents and phosphate, the adsorption process is significantly influenced by many factors including the pH, anions, organic acid, as well as the sorption conditions.

5.2.2.1 Effect of the P/La Value

In this study, the dosage of adsorbents is replaced by the molar ratio of phosphorus to lanthanum (P/La) for more accurately reflecting the nature of the problem. In most cases, the removal efficiency (RE) increases as the molar ratio of P/La descends until it reaches a peak RE value, which generally remains constant even if the value of P/La is descended (Koilraj and Sasaki 2017). Under the low loading of lanthanum, the phosphate ions cannot be completely captured by the lanthanum for providing less active sites for phosphate adsorption. When the maximum adsorption capacity is obtained, the quantity of the particles is sufficient to interact with the phosphate.

Table 5.2 Nanosized La-based nanomaterials for phosphate removal

Type	Adsorbent	La Content (Wt %)	P/La	pH_{pzc}	Size (nm)	S_{BET} ($m^2 \bullet g^{-1}$)	Experimental conditions	SC (mg $P \bullet g^{-1}$)	RE (%)	Model		References
										isotherm	kinetic	
/	La_2O_3	85.27	/	/	3 ~ 6	12	/	46.95	/	/	/	Xie et al. (2015)
La-clay mineral	La_{40}SBA-15	28.57	1.17		7.87 (pore)	326.0	[P] = 10 ~ 80 mg·L^{-1}; [La_{40}SBA-15] = 1 g·L^{-1}; T = 25 °C	20.08	40	Langmuir	Pseudo-second-order	Yang et al. (2011)
	La_{100}SBA-15	50.00	0.88		7.58 (pore)	227.0	[P] = 10 ~ 80 mg·L^{-1}; [La_{100}SBA-15] = 1 g·L^{-1}; T = 25 °C	45.63	95	Langmuir	Pseudo-second-order	Yang et al. (2011)
	La-clinoptilolite	4.01	0.17	/	18.65 (pore)	13.6	[P] = 5 ~ 240 mg·L^{-1}; [La-clinoptilolite] = 500 g·L^{-1}; T = 25 °C; pH = 8.0	1.49	99.45	Langmuir	Pseudo-second-order	Tu et al. (2016)
	LaAl-pillared clays	/	/	/	1.98 (basal spacing)		[LaAl-pillared clays] = 25 g·L^{-1}; T = 25 °C; pH = 5.0	8.90	/	Freundlich	Pseudo-first-order	Tian et al. (2009)
	La(III)-modified bentonite (NT-25La)	/	/	/	Less than 4 (pore)	115	[NT-25La] = 0.5 ~ 80 g·L^{-1}; T = 25 °C; pH = 6.0	14.0	90	Langmuir	/	Kuroki et al. (2014)
La-organics	FMS-0.02La	4.25	1.18	/	200 ~ 250	278.3	[P] = 50 mg·L^{-1}; [FMS-0.02La] = 1 g·L^{-1}; T = 25 °C	9.72	19	/	/	Huang et al. (2015a, b)
	FMS-0.10La	16.56	1.16	/	200 ~ 250	102.6	[P] = 50 mg·L^{-1}; [FMS-0.10La] = 1 g·L^{-1}; T = 25 °C	42.76	86	/	/	Huang et al. (2015a, b)
	MWCNTs-COOH-La	7.71	1.04	~5.0	20 ~ 40	140.0	[P] = 50 mg·L^{-1}; [MWCNTs-COOH-La] = 0.625 g/L; T = 25 °C	48.02	60	/	/	Zong et al. (2017)
	La_2O_3/PAN nanofibers	14	0.36	8.0	160 ~ 290	/	[P] = 20 ~ 80 mg·L^{-1}; [La_2O_3/PAN nanofibers] = 3.0 g·L^{-1}; T = 25 °C	10.89	28	/	/	He et al. (2016)
	Wheat straw-N-La	15.10	1.99	10.7	10 ~ 20	87.8	[P] = 5 ~ 80 mg·L^{-1}; [wheat straw-N-La] = 0.5 g·L^{-1}; T = 25 °C; pH = 6.2	67.10	94	Langmuir	/	Qiu et al. (2017)
	La-polystyrene networks	15.8	/	10.5	4.88 (pore)	24.42	/	/	/	/	Pseudo-second-order	Zhang et al. (2016)

(continued)

Table 5.2 (continued)

Type	Adsorbent	La Content (Wt %)	P/La	pH_{pzc}	Size (nm)	S_{BET} ($m^2 \bullet g^{-1}$)	Experimental conditions	SC (mg $P \bullet g^{-1}$)	RE (%)	Model		References
										isotherm	kinetic	
	$La(OH)_3$/porous carbon ($La_{0.1}$-PC)	/	0.936	/	/	308.9	/	12.52	/	Langmuir	/	Koilraj and Sasaki (2017)
	La-MOF-500	16.71	1.04	/	200 ~ 500	28.3	[P] = 40 ~ 100 mg·L^{-1}; [La-MOF-500] = 0.2 g·L^{-1}; T = 25 °C	173.8	/	Langmuir	Pseudo second-order	Zhang et al. (2017)
	3D graphene−La_2O_3	62.8	/	5.0	/		[3D graphene−La_2O_3] = 2 g·L^{-1}; T = 25 °C; pH = 6.2	82.6	/	/	Pseudo-second-order	Chen et al. (2015a, b)
La-metallic compound	HMS-1/5	22.44	/	4.4	500 ~ 600	420.38	[HMS-1/5] = 0.5 g·L^{-1}; T = 25 °C; pH = 5.0	47.89	/	Langmuir	Pseudo-second-order	Huang et al. (2014a, b)
	La_{200}-silica foams (La_{200}MOSF)	/	0.86	3 ~ 10	/	172	/	70.4	/	/	Pseudo-second-order	Yang et al. (2012)
	Fe_3O_4@SiO_2-La	11.17	/		10 ~ 40	47.73	[P] = 0 ~ 200 mg·L^{-1}; [Fe_3O_4@SiO_2-La] = 1 g·L^{-1}; T = 25 °C	27.80	99	Langmuir	/	Lai et al. (2016)

[a]Note: *P/La* Mole ratio of adsorbed Phosphate/La, S_{BET} Specific surface area, *RE* Removal efficiency, *SC* Sorption capacity;

However, even with the greater loading of lanthanum, there is some inferior adsorption capacity for different adsorbents, as shown in Table 5.2. This is probably due to the great S_{BET} and special pore size (Huang et al. 2014a, b; Tu et al. 2016).

5.2.2.2 Effect of pH Value

Generally, the process of adsorption is deeply affected by pH of solution which influences state of the presence of substances in the solution and the surface charge of adsorbent. So, pH value is a very important parameter, affecting the removal efficiency of phosphorus in water by lanthanum modified adsorbent.

Some studies have reported that the adsorption process of phosphate was strongly dependent on the pH value of solution (Zong et al. 2017; Huang et al. 2015a, b; Lai et al. 2016). Figure 5.4b presents that the adsorption capacity of MWCNTs-COOH-La changed very little within the pH range of 3.0 ~ 7.0. As pH reached 10.0, the adsorption capacity of MWCNTs-COOH-La (33.7 mg P g^{-1}) was reduced by 22%, as compared with the value at pH 3.0 (43.1 mg P g^{-1}) (Zong et al. 2017).

The distribution of phosphate species e.g., H_3PO_4, H_2PO^{4-}, HPO_4^{2-} and PO_4^{3-}, in aqueous medium is highly dependent on the variation of pH value, which associates closely to the dissociation equilibrium constants of these phosphate species, such as $pK_1 = 2.12$, $pK_2 = 7.21$, and $pK_3 = 12.67$ (Yang et al. 2014; Huang et al. 2014a, b).

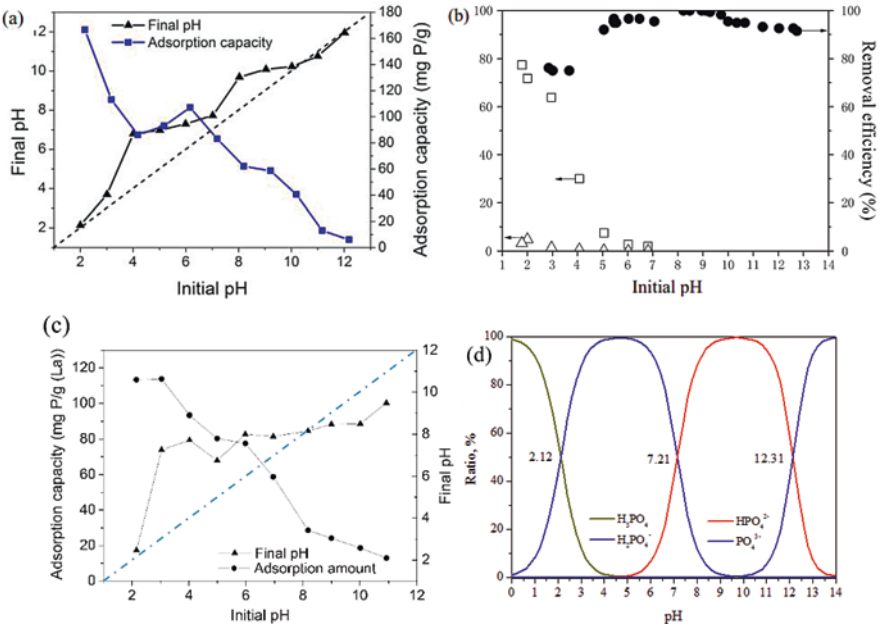

Fig. 5.4 Effect of pH value on phosphate adsorption of La-MOF-500 (**a**), Fe_3O_4/SiO_2-La (**b**) and La_2O_3-PAN fibers (**c**) and phosphate species of P (**d**) (Lai et al. 2016; Zhang et al. 2017)

So, a higher pH value causes the adsorbents surface to carry more negative charges and thus would more significantly repulse the negatively charged species in solution.

The increasing concentration of OH^- in alkaline solution will greatly compete for the active sorption sites with phosphate ions, resulting in a significant decrease in phosphate adsorption and adsorption process was inhibited by precipitation of lanthanum (III) hydroxides (Suzuki et al. 1989). On the other hand, the material would become negatively charged when solution pH is larger than the pH_{pzc} (point of zero charge), which could have the same charge as phosphate ions. Thus, the Donnan co-ion exclusion or electrostatic repulsive forces would be dominated in adsorption, which is favorable for the loaded phosphate desorption. In addition, the monovalent phosphate anion, $H_2PO_4^-$, has the greatest affinity for the adsorbent surface (Haghseresht et al. 2009).

We can see that there are four different chemical forms in different range of pH value. According to Schroeder, the affinity of adsorbent for anions mainly depends on the anion's valence and size (Schroeder 1984). The higher the valence and the smaller the hydrated ionic radius, the stronger is the adsorption.

The increase in pH value during the adsorption process further confirms the ligand-exchange mechanism involved in the phosphate adsorption process.

In the rough range of pH value (2.0 ~ 7.0), the lanthanum deposited on the adsorbents works as an active site, providing a great affinity to the monovalent phosphate species ($H_2PO_4^-$) (the predominant phosphate species), which have a higher affinity for La (Wu et al. 2007). Moreover, with the rise of pH value, an additional advantage in treating wastewater without post-treatment pH adjustments is revealed (Koilraj and Sasaki 2017).

Although the performance of La-based adsorbents has a decrease in condition of strong acids and alkalis, pH range (middle pH range) with high removal rate is the case of most wastewater or polluted natural water. However, as shown in Fig. 5.4c, d, the impact of pH values on both adsorbents assumes an opposite state of affairs. The possible reason is that different mechanisms which play a major role on whole reactions.

5.2.2.3 Effect of Coexisting Anions

There is no doubt that the co-existing anions, such as F^-, Cl^-, NO_3^-, CO_3^{2-} and SO_4^{2-}, which commonly occurring in natural waters or wastewater, are supposed to compete with phosphate ions for the active sites of adsorbents. So, the influences resulted by above anions are further evaluated by researches.

In order to reflect the impact more clearly, the effects of various anions in many literatures are summarized in Table 5.3.

With the increase of the concentration of coexisting anions, the adsorption of phosphorus decreased in different degrees. For example, the addition of foreign anions decreases the adsorption capacity of La_{100}SBA-15 by 27%, 30%, 14%, 40% and 12% for F^-, Cl^-, NO_3^-, CO_3^{2-} and SO_4^{2-}, respectively (Yang et al. 2011). In addition to carbonate ion, other particles would slightly retard the adsorption of phosphate.

Table 5.3 Comparison of the effect of phosphate adsorption capacities among the different anions

Type	Co-ion free Uptake (mg $P \cdot g^{-1}$)	Working conditions	Type	Decrease in the presence of coexisting anions (%)						References
				NO_3^-	F^-	Cl^-	SO_4^{2-}	CO_3^{2-}	HCO_3^-	
La-organics	~140	/	Sorption capacity	No	/	No	No	13	/	Zhang et al. (2017)
	11.6	[coexisting anion] = 20 mmol·L^{-1}	Sorption capacity	/	/	No	No	31	/	Koilraj and Sasaki (2017)
	~57	[coexisting anion] = 20 mmol·L^{-1}	Sorption capacity	26		~20.7	~24	/	~24.6	Zhang et al. (2016)
	82.6	[coexisting anion] = 8 g·L^{-1}	Removal efficiency	0	/	0	0	/	/	Chen et al. (2015a, b)
	82.6	[P] = 142 mg·L^{-1}; pH = 6.2;	Removal efficiency	13.5	/	20.0	10.9	/	/	Chen et al. (2015a, b)
La-clay minerals	20.76	[coexisting anion] = 0.01 Mol·L^{-1}	Sorption capacity	No	No	No	No	No	No	Huang et al. (2014a, b)
	20.76	[coexisting anion] = 0.1 Mol·L^{-1}	Sorption capacity	1–2	No	No	No	54.3	No	Huang et al. (2014a, b)
	1.93	[coexisting anion] = 0.5 mmol·L^{-1}	Removal efficiency	4.41		11.76	4.41		25.53	Tian et al. (2009)
La-silica	37.20	[coexisting anion] = 400 mg·L^{-1}	Sorption capacity	14	27	30	12	40	/	Yang et al. (2011)
	40.25	[coexisting anion] = 0.01 Mol·L^{-1}	Sorption capacity	1–2	No	No	1–2	31.4	/	Huang et al. (2015a, b)
	45.77	[coexisting anion] = 0.01 Mol·L^{-1}	Sorption capacity	~12	~1	~1	~1	~20	/	Huang et al. (2014a, b)
La-metallic	46.95	[coexisting $anion_{total}$] = 0.1 Mol·L^{-1}	Sorption capacity	7.1						Xie et al. (2015)
	27.8	[coexisting $anion_{total}$] = 0.01 Mol·L^{-1}	Removal efficiency	1.3	/	1.1	5.2	/	5.3	Lai et al. (2016)

From Table 5.3, we can see that the anion of CO_3^{2-} has the largest influence on the phosphate adsorption capacity. Because the initial pH of the solution with CO_3^{2-} is belong to alkaline, such as the pH of 0.1 mol·L^{-1} CO_3^{2-} is 11.6 or so. Under above condition, a large amount of OH^- is present, which competes with PO_4^{3-} for the adsorption active sites and hinders the ligand-exchange mechanism, thus lowering phosphate uptake more significantly (Huang et al. 2015a, b). Meanwhile, we can see that the concentration of carbonate (CO_3^{2-}) or bicarbonate (HCO_3^-) ions has a great negative effect on the adsorption capacity. This was maybe attributed to the lower solubility product constant (K_{sp}) of $La_2(CO_3)_3$ (3.98×10^{-34}) compared with that of $LaPO_4$ (3.7×10^{-23}), which supported the alteration of the formed $LaPO_4$ to $La_2(CO_3)_3$ (Huang et al. 2014a, b).

But there is a big difference in terms of HCO_3^- ions between this two references (Zhang et al. 2016; Tian et al. 2009). The possible reason is the effect of structure or zeta potential of material itself (Edzwald et al. 1976). If ion exchange played a significant role in the adsorption process, then the introduction of coexisting anions would have cut down the amount of phosphate adsorbed. Furthermore, the orders of the effect of various anions on the phosphate adsorption may be related with affinity of adsorbents toward anions (Schroeder 1984; Tian et al. 2009).

5.2.2.4 Effect of Temperature

Temperature is an important parameter among several chemical and physical reactions. In nano-La typed adsorbents, the pore structure of matrix materials, even process of chemical adsorption is deeply affected by the temperature value. Large pore size of adsorbents contributes to the adsorption of P species (Yang et al. 2011).

5.2.2.5 Adsorption–Desorption Cycle

In many studies, batch adsorption-desorption cycles are always carried out to investigate the repeated property of adsorbents. To a certain extent, desorption of P from La-adsorbents was difficult, for the forceful interaction between La sites and P.

Typically, the means of regeneration are divided into alkali treatment and acid treatment. The phosphate–La compounds to give soluble La^{3+} and H_3PO_4 were gradually dissolved by acid treatment (0.5 M HCl). The reusability of fresh nano-La typed adsorbents mainly depends on the amount of PO_4^{3-} ions desorbed from used sample. From the Table 5.4, unfortunately, we can see that the 90% of capacity of materials can still be maintained after the regeneration treatment, which indicates that the reusability of the materials is relatively satisfactory. In addition, the process of regeneration treatment will result in a caustic wastewater stream that contains high P, to which the calcium containing chemicals may be added into the alkaline wastewater stream for converting phosphate into calcium biphosphate, used as calcium phosphate fertilizer (Urano et al. 1992; Midorikawa et al. 2008). The remaining alkali solution could be neutralized by adding sulfuric acid before further reused

Table 5.4 Regeneration methods and regeneration efficiency of materials

Adsorbent	Desorption agent	Regeneration process	Desorption (%)	Re-adsorption (%)	Cycles	References
Wheat straw-N-La	NaOH	NaOH-NaCl (10%–5%) solution	85	90	10	Qiu et al. (2017)
La_2O_3	NaOH	12.5 M NaOH at 140 °C at a liquid and solid ratio of 6 mL·g^{-1} for a duration of 5 h	96.12	100	1	Xie et al. (2015)
La_2O_3	Oxalic acid	0.5 M oxalic acid at room temperature at a liquid/solid ratio of 80 mL·g^{-1}	98.75	100	1	Xie et al. (2015)
HMS-1/5	HCl	0.5 M HCl solution at room temperature at a liquid/solid ratio of 1 L·g^{-1} for 24 h	100	99	1	Huang et al. (2014a, b)
La_5EV	NaOH	0.10 M NaOH solution for 48 h	88.5	70	3	Huang et al. (2014a, b)
LaAl- pillared clays	NaOH	0.1 M NaOH solution for 12 h	–	91–96	6	Tian et al. (2009)
La-vesuvianite	HNO_3	25 mL of 5% HNO_3 with the used sample for 24 h (soaked and stirred)	100	100	1	Li et al. (2009)
Fe_3O_4@ SiO_2-La	NaOH	3.0 M NaOH solution and 50 °C	95.1		/	Lai et al. (2016)
La-MOF-500	NaOH	300 mL 0.1 M NaOH for 4 h, then rinsed to pH =7 with DI water and dried	/	18	/	Zhang et al. (2017)
La-MOF-500	Calcination	500 °C	/	34	/	Zhang et al. (2017)

as desorption reagent for several times. Of course, for the environmental-friendly adsorbents (e.g. chitosan or clay, and so on), they can be used as a resource of fertilizer in agriculture directly.

Overall, in spite of the promising future of the nano-La based materials in environmental technologies, there are some issues and challenges that need to be overcome before large scale development of the nano-La based materials. For example, these environmental factors (water flow, hydraulic pressure) should be given significant attention when considering the application of La modified adsorbents in eutrophication control; the biotoxicity of the material itself needs to be further studied; for non-recyclable adsorbents, the status about long-term desorption needs to be studied.

5.3 Removal of Harmful Algae by Nano-photocatalysts in Water

All things are relative. When concentration of algal is at a normal level, the virtuous circulation of aquatic ecosystems is guaranteed, and the shades for hydrobiontes from the sunlight are also provided. However, the high concentration of algae will be disastrous, as their huge amount will exhaust the oxygen supply through respiration and releasing carbon dioxide during nighttime.

Therefore, when algal blooms erupt, measures are taken. In general, mechanical salvage is universally adopted, but this method is time-consuming and laborious, and often does not achieve good results. In recent years, with the development of photocatalytic technology (simple and low cost), a new and effective solution to remove algae from eutrophication water is provided.

5.3.1 Nano-photocatalysts

In the photocatalytic catalyst for algae removal, nano TiO_2 has been widely studied because of its chemical stability, non-toxic, low cost and high photocatalytic activity. Meanwhile, other types of nano-photocatalysts have emerged, such as ZnO, $AgBiO_3$, and so forth.

But in practice, photocatalysts also have their own defects. Firstly, high recombination rate of electrons and holes produced by light and low quantum efficiency, both greatly reduce the photocatalytic activity. Secondly, TiO_2 has wide bandgap. Theoretically, only ultraviolet light can stimulate valence band electrons to transition to conduction band. And the ultraviolet light accounts for only 4% of the solar radiation, so the utility rate of the sunlight is low, and the artificial ultraviolet light is relatively expensive and the use range is also limited.

From the Table 5.5, the removal of algae by nano-photocatalysts reached 90% within 2 h under UV light. However, the removal efficiency under visible light needs to be improved in the future.

Table 5.5 Performance of nano-photocatalyst for removing algae

Materials	Particle Size	Contact time	Algae	initial concentration (cells·mL^{-1})	Working conditions	Removal rate	References
Montmorillonite/ ($CuO + Fe_2O_3$)	/	20 min	M. aeruginosa	53 mg·L^{-1}	pH = 6.8, 1 g·L^{-1},	94.8%	Gao et al. (2009)
Ag-TiO_2	7–14 nm	60 min	A. carterae	$(1 \pm 0.1) \times 10^5$	UV, 40 W,	99%	Rodríguez-González et al. (2010)
Ag-TiO_2	7–14 nm	40 min	T. suecica	$(2.5 \pm 0.2) \times 10^5$	UV, 40 W,	100%	Rodríguez-González et al. (2010)
Cu_2O-montmorillonite	5–10 nm	180 min	M. aeruginosa	2.8×10^7	Visible light, 400 mg·L^{-1},	90.4%	Gu et al. (2016a, b)
ZnO–montmorillonite	30 nm	60 min	M. aeruginosa	2.8×10^5	UV_λ = 365 nm, 300 W, 50 mg·L^{-1},	95%	Gu et al. (2015)
N,P doped TiO_2/graphite carbon layer	50 nm	9 h	M. aeruginosa	2.7×10^6	$\lambda > 380$ nm	98.15%	Wang et al. (2017)
Zn–Fe LDHs	0.75 nm	150 min	M. aeruginosa	2.8×10^5	Visible light, 250 mg·L^{-1},	80.6%	Gu et al. (2016a, b)
$AgBiO_3$	~500 nm	96 h	M. aeruginosa	~1.0×10^6	/	65.69%	Yu et al. (2010)

5.3.2 *Mechanism of Photocatalytic Removal of Algae*

The principle of photocatalysis lies in the production of many free radicals, which have the effect of killing algae. As shown below.

$$\text{pholocatalyst} + h\vartheta \rightarrow e^- + h^+ \tag{5.6}$$

$$OH^- + h^+ \rightarrow \cdot OH \tag{5.7}$$

$$O_2 + e^- \rightarrow \cdot O_2^- \tag{5.8}$$

$$\cdot O_2^- + h^+ \rightarrow HO_2 \cdot \tag{5.9}$$

$$HO_2 \cdot + HO_2 \cdot \rightarrow H_2O_2 + O_2 \tag{5.10}$$

$$H_2O_2 + e^- \rightarrow OH^- + \cdot OH \tag{5.11}$$

$$H_2O_2 + \cdot O_2^- \rightarrow OH^- + \cdot OH + O_2 \tag{5.12}$$

When the energy of light irradiated to the surface of the catalyst is higher than the band gap (E_g) of the semiconductor, the electrons in the semiconductor will be excited to move from the valence band to the conduction band. An electron-hole pair with strong activity is formed and further induces a series of redox reactions (6–12).

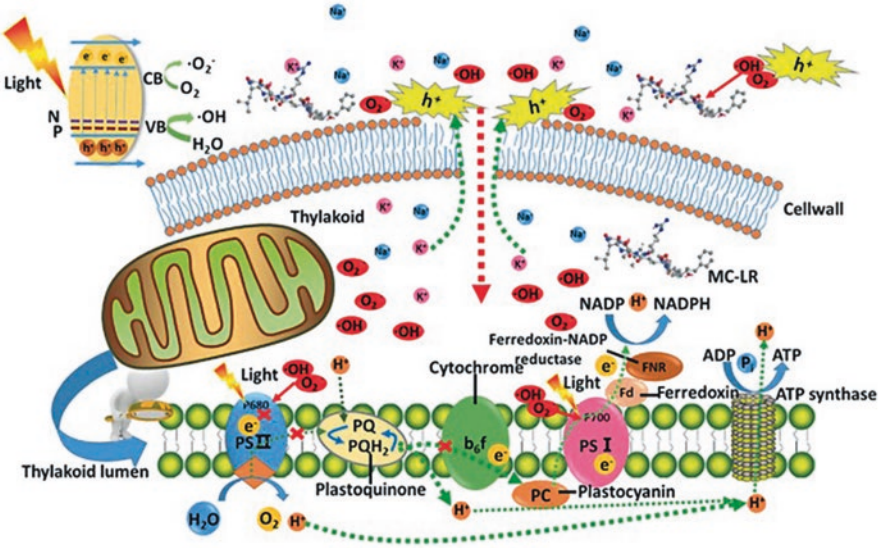

Fig. 5.5 Schematic of the possible reaction mechanism of the photocatalyst (from (Wang et al. 2017))

From Fig. 5.5, we can see that the algae was destructed by the radicals (·OH, h^+ and $\cdot O^{2-}$ and so on) produced by photocatalyst and the process can be divided into three steps: first, cell walls and membranes were destroyed (The ROS can cause irreversible damage to the membrane protein, which results in electrolyte leaking; after which, the conductivity of the solution increases); Then, the photosynthetic system was damaged; Finally, degradation of the metabolic products was achieved by photocatalyst (Yu et al. 2010).

5.4 Removal of Microcystins in Water

Algae bloom due to eutrophication in aquatic environments and associated microcystins contamination are increasingly reported worldwide (Carmichael et al. 2001). The adverse effects of cyanobacterial toxins were first reported as stock deaths at Lake Alexandrina, South Australia, in 1878. Since then, poisoning incidents of microcystins in animals and humans have been widely reported around the world. Microcystins can be accumulated in aquatic organisms and transferred to higher trophic levels through the food chain, representing a health hazard to animals and humans (Chen et al. 2016; Florczyk et al. 2014).

Algal toxins are mainly produced from cyanobacteria, including microcystins (MCs), neurotoxins, nodularins, hepatotoxins, anatoxins alpha, paralytic shellfish poisoning, and so on. At present, the research targets of algae toxins mainly focus on microcystins. MC belongs to the cyclic seven peptide of liver toxins and has many isomers, among which the most common are MC-LR, MC-RR, MC-YR (L, R, Y as leucine, arginine and tyrosine respectively). Until now, nearly 90 variants of microcystins have been discovered (Zhang et al. 2010).

MC-LR (LD_{50} = 50 $g{\cdot}kg^{-1}$) exhibits higher lethality than the venom of dangerous snakes such as cobra (LD_{50} = 500 $g{\cdot}kg^{-1}$) (Richardson 2007). In addition, MCs are extremely stable and resistant to chemical hydrolysis or oxidation at nearly neutral pH values, and they may persist for months or even years in natural water. When MC-LR enters the human body, it can produce a large number of hepatic toxins in a short time, and inhibit the production of protein phosphatase, thus causing tumor lesions (Wiegand and Pflugmacher 2005).

Because cyanobacterial toxins have hepatotoxicity, neurotoxicity, genotoxicity, embryonic toxicity, and carcinogenicity, the residual algal toxins in drinking water can cause serious health risks to humans (Meneely and Elliott 2013; Fang 2013). The limiting concentration for algal toxins in drinking water is less than 1.0 $ug{\cdot}L^{-1}$ in China and World Health Organization.

The maximum possible length of the MC-LR molecule is 2.94 nm (Sathishkumar et al. 2010a, b). MC-LR contains five nonproteinogens and two substitutions of leucine (L) and arginine (R) at positions 2 and 4, which is the most toxic species, as shown in Fig. 5.6.

In these microcystins, the MC-LR is the most common and toxic variant of the group of microcystins (MCs) produced during the formation of harmful

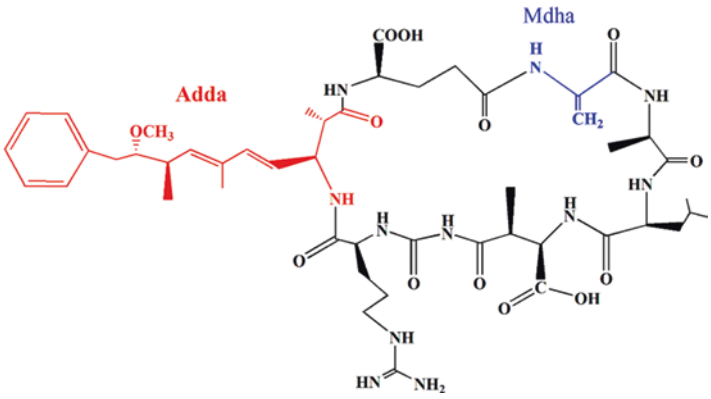

Fig. 5.6 Structure diagram of MC-LR

cyanobacterial blooms. In this paper, therefore, a brief summary on the current nanotechnologies of dealing with MC-LR is made to provide some guidance.

5.4.1 Doped TiO_2 Nano-pholocatalyst

As we all know, photocatalytic materials have been extensively studied in recent years and have great prospects on degradation of organic pollutant, including phenolic, chlorine, antibiotic and so forth (Grabowska et al. 2012). Similarly, MCs belong to organic macromolecules and could be degraded by photocatalysis (Triantis et al. 2012).

Although TiO_2 has a high photocatalytic activity under UV light, its limited photocatalytic activity in visible light is still one of its main drawbacks. Therefore, it is of great interest to find a way to extend the absorption wavelength range of TiO_2 to the visible region. Actually, a huge emphasis has been put all over the world to generate a visible light active TiO_2.

But conventional TiO_2 photocatalyst can only utilize the light with wavelengths shorter than 388 nm (UV range) due to its wide band gap (e.g. Eg $\approx$ 3.2 eV for anatase). These elements (C, N, S, F) utilized as dopants to narrow the band gap or form intra band gap of TiO_2 materials and decrease the required activation energy (Barolo et al. 2012). For example, N doping can achieve band gap narrowing through substitution lattice sites by mixing of N2p with O2p states in the valence band (Asahi et al. 2001). In the case of sulfur doping, sulfur substitutes either the oxygen as an anion or the titanium as cations. The overlap of sulfur 3p states and oxygen 2p states facilitates the visible light catalytic activity of S-doped TiO_2. For low concentration of carbon doping, Di Valentin et al. have reported that carbon atoms prefer to be interstitial and substitutional to Ti atoms under oxygen-rich conditions, whereas prefer to be substitutional to O under anoxic conditions (Tachikawa et al. 2004, Di Valentin et al. 2005).

Table 5.6 Parameters and removal rates of MC-LR from different doped TiO_2

Adsorbent	Wavelengths	S_{BET} ($m^2 \bullet g^{-1}$)	Working condition	Removal	References
P25	320 ~ 400 nm	/	[MC-LR] = 10 mg·L^{-1}; dose = 200 mg·L^{-1}; irradiation = 10 min;	100%	Fotiou et al. (2015)
P25	>420 nm	/	[MC-LR] = 0.5 ug·L^{-1}; dose = 500 mg·L^{-1}; irradiation = 5 h;	12.2%	El-Sheikh et al. (2014)
C doped TiO_2	/	103	[MC-LR] = 500 μg·L^{-1}; 1 h; 7.81 × 10^{-5} W·cm^{-2}; pH = 5.7	550.0 μg·g^{-1}	Likodimos et al. (2013)
C doped TiO_2	410 ~ 420 nm	/	[MC-LR] = 2 g·L^{-1}; dose = 200 g·L^{-1}; irradiation = 5 h;	55%	Fotiou et al. (2016)
N doped TiO_2	Solar irradiation	/	[MC-LR] = 10 mg·L^{-1}; dose = 450 mg·L^{-1}; irradiation = 4 h;	100%	Fotiou et al. (2015)
S doped TiO_2	/	179	/	630.4 μg·g^{-1}	Likodimos et al. (2013)
S doped TiO_2	>420 nm		[MC-LR] = 500 μg·L^{-1}; dose = 200 mg·L^{-1}; irradiation = 5 h;	60%	Changseok et al. (2011)
N-F doped TiO_2	/	136	/	187.5 μg·g^{-1}	Likodimos et al. (2013)
S-N-C doped TiO_2	/	85.1	/	100%	El-Sheikh et al. (2014)
S-N-C doped TiO_2	/	135.9	Visible light	75% in 5 h	Zhang et al. (2014)

For example, Likodimos et al. reported that the band gap (~3.2 eV) of anatase TiO_2 phase achieved a marked decline (2.9, 2.8 and 2.7 eV) by doping the non-metal elements (N-F, S and C) respectively (Likodimos et al. 2013).

From the Table 5.6, we can see that with the doping of elements, the photocatalytic properties of the materials are improved under visible light. There are three reasons for the high photodegradation rate of doped-TiO_2. First, the high adsorption rate of doped-TiO_2 results in a higher photocatalytic potential. Second, electrons could be promoted from the VB to the CB more easily, resulting in the formation of energized holes on the surface of the TiO_2. Third, doped elements can impede electron–hole recombination and enhance the efficacy of photocatalytic degradation. With the element doped, this behavior could be ascribed to a red-shift of the energy band gap to the visible range lower than 3.2 eV, justifying visible light photocatalytic activity during MC-LR degradation (El-Sheikh et al. 2014; Pelaez et al. 2016).

5.4.2 *Photodegradation Mechanism of Photocatalyst*

Photocatalyst produces electron transition under light condition, forming holes and electrons, and then producing a lot of free radical groups to oxidize and degrade pollutants. Through the analysis of free radicals, the main action of free radicals was obtained, and the intermediate products were analyzed by Mass Spectrometric analysis, and the mechanism of degradation was obtained in detail as shown in Fig. 5.7.

It has been determined that degradation of MC-LR occurs at four sites of the structure: the aromatic ring, the methoxy group, conjugated double bond of the Adda group and the cyclic structure of the Mdha amino acid (Antoniou et al. 2008).

In general, The proposed pathways of photocatalytic degradation of MC-LR indicated that the conjugated double bond and methoxy group in Adda, and the conjugated system in Mdha are liable to be attacked by •OH (Su et al. 2013). As shown in Fig. 5.7, the conjugated carbon double bonds of Adda were attacked by hydroxyl radicals presented by photocatalyst (pink area) and converted to HO-C-OH structure and further oxidation. The formed aromatic ring and double bonds will be further oxidized to another substance or directly mineralized. After breakdown of the conjugated system in Mdha, the carboxyl group and amino group of the peptides are hydrolyzed. Subsequently, the side chain of the amino acid could be oxidized and mineralized. The Adda chain is deduced to be destroyed and separated from the heptapeptides to produce alkyl derivatives (Wu et al. 2017a, b).

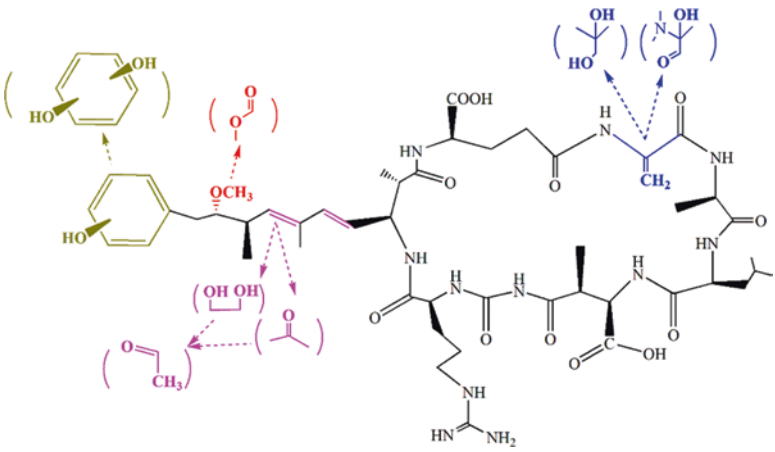

Fig. 5.7 Brief diagram of degradation pathway of MC-LR by photocatalyst

Table 5.7 Comparison of adsorption capacities of MC-LR with different adsorbents

Adsorbents	Particle Size	Pore size	Contact time	pH	Adsorption capacity	Model	References
Fe_3O_4@nSiO_2@mSiO_2 microspheres	200 nm	2.3 nm	5.0 min	7.0	160 mg·g^{-1}	/	Deng et al. (2008)
Mesoporous carbons	4.5 × 1.9 mm	2.8 to 5.8 nm	4 h	/	526 mg·g^{-1}	Langmuir	Teng et al. (2013)
PPy/Fe_3O_4	50–100 nm	/	10 min	7.0	301.11 mg·g^{-1}	Langmuir	Hena et al. (2016)
Carbon nanotubes	2–60 nm	/	8 h	7.0	14.8 mg·g^{-1}	/	Yan et al. (2006)
Graphene oxide	1.0 nm	/	5 min	5.0	1.69 mg·g^{-1}	Langmuir	Pavagadhi et al. (2013)
Peat	/	1–13.3 nm	30 min	3.0	0.286 mg·g^{-1}	Langmuir	Sathishkumar et al. (2010a, b)
γ-Fe_2O_3	10–30 nm	/	48 h	4.4	2.7264 mg·g^{-1}	/	Lee and Walker (2011)
N-doped carbon xerogel	/	4.1 nm	30 min	/	1.9162 mg·g^{-1}	Langmuir	Wu et al. (2017a, b)
Mesoporous carbons	/	8.5–14 nm	/	/	35.67 mg·g^{-1}	Langmuir	Park et al. (2017)
Rattle-type magnetic carbon shell	~600 nm	2.7 nm	5 min	7.0	166.67 mg·g^{-1}	/	Zhang and Jiang (2011)
Mpg-C_3N_4–H^+	/	14.68 nm	15 min	7.0	2.361 mg·g^{-1}	Langmuir	Huang et al. (2015a, b)
Porous activated semi-cokes	/	2–20 nm	24 h	/	8.43 mg·g^{-1}	Langmuir	Chen et al. (2015a, b)

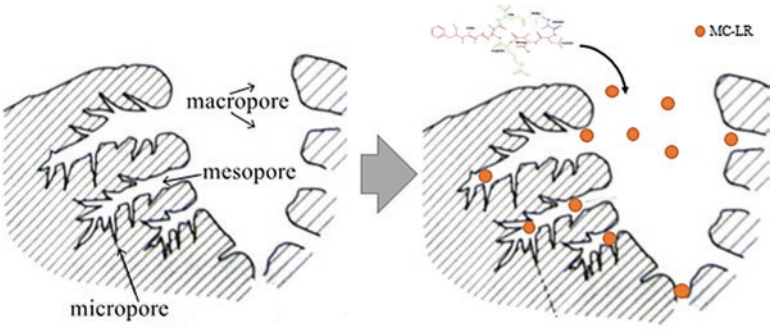

Fig. 5.8 Adsorption model illustration of MC-LR molecules on nano-adsorbents

5.4.3 Nanosized Adsorbents

After many depth studies, it was found that the pore size of the adsorbent was associated with the size of the microcystin. The largest volume of mesopores (pore diameter in the range of 2 ~ 50 nm) were shown to be the most efficient as shown in the Table 5.7 (Donati et al. 1994).

From the Table 5.7, we can obviously see that the adsorption model is basically consistent with Langmuir and the pore size is mainly between 2 and 50 nm for the adsorbent with high adsorption capacity (Fig. 5.8). In addition, MC-LR molecules, with several carbonyl and carboxyl groups, also have a strong affinity toward the metals (Xia et al. 2013; Vimont et al. 2006).

5.4.4 Other Combined Means

Other scholars have combined the advantages of adsorption and degradation technology. For example, Wei et al. have synthesized carbon-nanotube-based sandwich-like hollow fiber membranes, which present three layer structure, the outer layer is a carbon nanotube, and the center is PVDF (40–60 nm CNT layer-PVDF-60-100 nm CNT layer). The removal of MC-LR is achieved by accessing the voltage of the 2 ~ 3 V (Wei et al. 2017). A marked effect has been achieved by Combining ultrafiltration (UF) membrane combined with coagulation and flocculation and powdered activated carbon for removing intra- and extracellular microcystin (Şengül et al. 2018). The functional bentonite supported Fe/Pd nanoparticles (B-Fe/Pd) was used to remove microcystin-LR (MC-LR) and the batch experiments showed that 96.86% of MC-LR was removed using B-Fe/Pd, while only 81.76% and 10.06% of MC-LR were removed using Fe/Pd nanoparticles and bentonite after degrading 3 h (Wang et al. 2014).

5.5 Conclusions

In summary, with the development of nanotechnology, more and more various types of nanomaterials are have been designed, synthesized and employed into eutrophication bodies, which have been well treated and repaired. In this review, the application of nanomaterials was described from phosphorus removal, algae blooms removal, and Microcystin-LR removal, respectively. The advances of nanomaterials lie in their large specific surface areas, which facilitate the provision of more active sites and enhance their ability to remove pollutants.

In terms of the removal of P from eutrophication, the main means of participation of nanotechnology is adsorbent. In this paper, La-based nano-adsorbent are summarized. In the nanometer field, the adsorption technology occupies the main position because of its feasibility and simplicity.

Additionally, for the removal of algae cell from the water, means of nanomaterials consists of adsorption and inactivation. However, what is disturbing is that when the cells are broken, the intracellular algae toxins would release into the water to increase the concentration of algal toxins in the water, which results in bigger problem. So, the current technologies focus on the strong adsorption capacity for adsorbents with nanostructure (size or pore) or degradation of both cells and intracellular pollutant such as nano-photocatalyst (TiO_2, ZnO, MoS, g-C_3N_4, and so on.).

For removal of algal toxin from water, more and more scholars are concerned about something that can be completely harmless, such as photocatalysis, Fenton-like reaction and so on. And in recent years, photocatalytic technology has been developed continually because of its high reaction activity, mild reaction condition and high mineralization rate. However, in view of the shortcomings of existing catalysts such as high carrier recombination rate and narrow range of photo response, it is of importance to select and optimize the catalyst.

Overall, nanomaterials play an important role in algae bloom. Besides, scale-up studies are put on the agenda before these methods are considered as economically feasible and practical sustainable alternatives in algae bloom control. Moreover, the current practical applications of nanomaterials will promote the birth of more highly efficient nanomaterials with unexpected performances, by which beauty of the world environment will be made.

Acknowledgments This work was supported by the National Natural Science Foundation of China (Grant No. 51778618), which is greatly acknowledged.

References

Antoniou MG, Shoemaker JA, de la Cruz AA, Dionysiou DD (2008) LC/MS/MS structure elucidation of reaction intermediates formed during the TiO2 photocatalysis of microcystin-LR. Toxicon 51(6):1103–1118. https://doi.org/10.1016/j.toxicon.2008.01.018

Asahi R, Morikawa T, Ohwaki T, Aoki K, Taga Y (2001) Visible-light photocatalysis in nitrogen-doped titanium oxides. Science 293(5528):269–271. https://doi.org/10.1126/science.1061051

Barolo G, Livraghi S, Chiesa M, Paganini MC, Giamello E (2012) Mechanism of the Photoactivity under visible light of N-doped titanium dioxide. Charge carriers migration in irradiated N-TiO2 investigated by Electron paramagnetic resonance. J Phys Chem C 116(39):20887–20894. https://doi.org/10.1021/jp306123d

Barrado-Moreno MM, Beltrán-Heredia J, Martín-Gallardo J (2017) Degradation of microalgae from freshwater by UV radiation. J Ind Eng Chem 48:1–4. https://doi.org/10.1016/j.jiec.2016.12.030

Carmichael WW, Azevedo SM, An JS, Molica RJ, Jochimsen EM, Lau S, Rinehart KL, Shaw GR, Eaglesham GK (2001) Human fatalities from cyanobacteria: chemical and biological evidence for cyanotoxins. Environ Health Perspect 109(7):663–668

Changseok H, Miguel P, Vlassis L, Kontos AG, Polycarpos F (2011) Innovative visible light-activated sulfur doped Ti02 films for water treatment. Appl Catal B Environ 107:77–87. https://doi.org/10.1016/j.apcatb.2011.06.039

Chen M, Huo C, Li Y, Wang J (2015a) Selective adsorption and efficient removal of phosphate from aqueous medium with graphene-lanthanum composite. ACS Sustain Chem Eng 4(3):1296–1302. https://doi.org/10.1021/acssuschemeng.5b01324

Chen Y, Zhang X, Liu Q, Wang X, Xu L (2015b) Facile and economical synthesis of porous activated semi-cokes for highly efficient and fast removal of microcystin-LR. J Hazard Mater 299:325–332. https://doi.org/10.1016/j.jhazmat.2015.06.049

Chen L, Chen J, Zhang X, Xie P (2016) A review of reproductive toxicity of microcystins. J Hazard Mater 301:381–399. https://doi.org/10.1016/j.jhazmat.2015.08.041

Chouyyok W, Wiacek RJ, Pattamakomsan K, Sangvanich T, Grudzien RM, Fryxell GE, Yantasee W (2010) Phosphate removal by anion binding on functionalized Nanoporous sorbents. Environ Sci Technol 44(8):3073–3078. https://doi.org/10.1021/es100787m

Copetti D, Finsterle K, Marziali L, Stefani F, Tartari G, Douglas G, Reitzel K, Spears BM, Winfield IJ, Crosa G, D'Haese P, Yasseri S, Lürling M (2016) Eutrophication management in surface waters using lanthanum modified bentonite: a review. Water Res 97:162–174. https://doi.org/10.1016/j.watres.2015.11.056

Delaney P, Mcmanamon C, Hanrahan JP, Copley MP, Holmes JD (2011) Development of chemically engineered porous metal oxides for phosphate removal. J Hazard Mater 185:382–391. https://doi.org/10.1016/j.jhazmat.2010.08.128

Deng Y, Qi D, Deng C, Zhang X, Zhao D (2008) Superparamagnetic high-magnetization microspheres with an Fe3O4@SiO2 Core and perpendicularly aligned mesoporous SiO2 Shell for removal of microcystins. J Am Chem Soc 130(1):28–29. https://doi.org/10.1021/ja0777584

Di Valentin C, Pacchioni G, Selloni A (2005) Theory of carbon doping of titanium dioxide. Chem Mater 17(26):6656–6665. https://doi.org/10.1021/cm051921h

Donati C, Drikas M, Hayes R, Newcombe G (1994) Microcystin-LR adsorption by powdered activated carbon. Water Res 28(8):1735–1742

Edzwald JK, Toensing DC, Leung CY (1976) Phosphate adsorption reactions with clay minerals. Environ Sci Technol 10(5):485–490. https://doi.org/10.1021/es60116a001

El-Sheikh SM, Zhang G, El-Hosainy HM, Ismail AA, O'Shea KE, Falaras P, Kontos AG, Dionysiou DD (2014) High performance sulfur, nitrogen and carbon doped mesoporous anatase-brookite TiO2 photocatalyst for the removal of microcystin-LR under visible light irradiation. J Hazard Mater 280:723–733. https://doi.org/10.1016/j.jhazmat.2014.08.038

Epe TS, Finsterle K, Yasseri S (2017) Nine years of phosphorus management with lanthanum modified bentonite (Phoslock) in a eutrophic, shallow swimming lake in Germany. Lake Reservoir Manag 33(2):119–129

Fang D (2013) Nodularins in poisoning. Clin Chim Acta 425:18–29. https://doi.org/10.1016/j.cca.2013.07.005

Florczyk M, Łakomiak A, Woźny M, Brzuzan P (2014) Neurotoxicity of cyanobacterial toxins. Environ Biotechnol 10(1):26–43. https://doi.org/10.14799/ebms246

Fotiou T, Triantis TM, Kaloudis T, Hiskia A (2015) Evaluation of the photocatalytic activity of TiO2 based catalysts for the degradation and mineralization of cyanobacterial toxins and water off-odor compounds under UV-A, solar and visible light. Chem Eng J 261:17–26. https://doi.org/10.1016/j.cej.2014.03.095

Fotiou T, Triantis TM, Kaloudis T, O'Shea KE, Dionysiou DD, Hiskia A (2016) Assessment of the roles of reactive oxygen species in the UV and visible light photocatalytic degradation of cyanotoxins and water taste and odor compounds using C–TiO2. Water Res 90:52–61. https://doi.org/10.1016/j.watres.2015.12.006

Gao Z, Penga X, Zhang H, Luan Z, Fan B (2009) Montmorillonite–Cu(II)/Fe(III) oxides magnetic material for removal of cyanobacterial Microcystis aeruginosa and its regeneration. Desalination 247:337–345. https://doi.org/10.1016/j.desal.2008.10.006

Grabowska E, Reszczyńska J, Zaleska A (2012) Mechanism of phenol photodegradation in the presence of pure and modified-TiO2: a review. Water Res 46(17):5453–5471. https://doi.org/10.1016/j.watres.2012.07.048

Gu N, Gao J, Wang K, Yang X, Dong W (2015) ZnO–montmorillonite as Photocatalyst and Flocculant for inhibition of cyanobacterial bloom. Water Air Soil Pollut 226:136. https://doi.org/10.1007/s11270-015-2407-5

Gu N, Gao J, Li H, Wu Y, Ma Y, Wang K (2016a) Montmorillonite-supported with Cu2O nanoparticles for damage and removal of Microcystis aeruginosa under visible light. Appl Clay Sci 132–133:79–89

Gu N, Gao J, Wang K, Li B, Dong W, Ma Y (2016b) Microcystis aeruginosa inhibition by Zn–Fe–LDHs as photocatalyst under visible light. J Taiwan Inst Chem Eng 64:189–195. https://doi.org/10.1016/j.jtice.2016.04.016

Haghseresht F, Wang S, Do DD (2009) A novel lanthanum-modified bentonite, Phoslock, for phosphate removal from wastewaters. Appl Clay Sci 46(4):369–375. https://doi.org/10.1016/j.clay.2009.09.009

Hartmann NB, Von der Kammer F, Hofmann T, Baalousha M, Ottofuelling S, Baun A (2010) Algal testing of titanium dioxide nanoparticles—testing considerations, inhibitory effects and modification of cadmium bioavailability. Toxicology 269(2–3):190–197. https://doi.org/10.1016/j.tox.2009.08.008

He J, Wang W, Shi W, Cui F (2016) La2O3 nanoparticle/polyacrylonitrile nanofibers for bacterial inactivation based on phosphate control. RSC Adv 6(101):99353–99360. https://doi.org/10.1039/C6RA22374E

Hena S, Rozi R, Tabassum S, Huda A (2016) Simultaneous removal of potent cyanotoxins from water using magnetophoretic nanoparticle of polypyrrole: adsorption kinetic and isotherm study. Environ Sci Pollut R 23(15):14868–14880. https://doi.org/10.1007/s11356-016-6540-5

Huang W, Li D, Yang J, Liu Z, Zhu Y, Tao Q, Xu K, Li J, Zhang Y (2013) One-pot synthesis of Fe(III)-coordinated diamino-functionalized mesoporous silica: effect of functionalization degrees on structures and phosphate adsorption. Microporous Mesoporous Mater 170:200–210. https://doi.org/10.1016/j.micromeso.2012.10.027

Huang W, Li D, Liu Z, Tao Q, Zhu Y, Yang J, Zhang Y (2014a) Kinetics, isotherm, thermodynamic, and adsorption mechanism studies of La(OH)3-modified exfoliated vermiculites as highly efficient phosphate adsorbents. Chem Eng J 236:191–201. https://doi.org/10.1016/j.cej.2013.09.077

Huang W, Zhu Y, Tang J, Yu X, Wang X (2014b) Lanthanum-doped ordered mesoporous hollow silica spheres as novel adsorbents for efficient phosphate removal. J Mater Chem A 2:8839–8848. https://doi.org/10.1039/c4ta00326h

Huang C, Zhang W, Yan Z, Gao J, Liu W (2015a) Protonated mesoporous graphitic carbon nitride for rapid and highly efficient removal of microcystins. RSC Adv 5:45368–45375. https://doi.org/10.1039/c5ra01415h

Huang W, Yu X, Tang J, Zhu Y, Zhang Y, Li D (2015b) Enhanced adsorption of phosphate by flower-like mesoporous silica spheres loaded with lanthanum. Microporous Mesoporous Mater 217:225–232. https://doi.org/10.1016/j.micromeso.2015.06.031

Huang W, Zhang Y, Li D (2017) Adsorptive removal of phosphate from water using mesoporous materials: A review. J Environ Manag 193:470–482. https://doi.org/10.1016/j.jenvman.2017.02.030

Kasp L, Jona N, Fred N, Kjel N, Henn N (2005) Lake restoration by dosing phosphorus in the sediment. Environ Sci Technol 39:4134–4140. https://doi.org/10.1021/es0485964

Koilraj P, Sasaki K (2017) Selective removal of phosphate using La-porous carbon composites from aqueous solutions: batch and column studies. Chem Eng J 317:1059–1068. https://doi.org/10.1016/j.cej.2017.02.075

Kuroki V, Bosco GE, Fadini PS, Mozeto AA, Cestari AR (2014) Use of a La(III)-modified bentonite for effective phosphate removal from aqueous media. J Hazard Mater 274:124–131. https://doi.org/10.1016/j.jhazmat.2014.03.023

Lai L, Xie Q, Chi L, Gu W, Wu D (2016) Adsorption of phosphate from water by easily separable Fe3O4 @SiO2 core/shell magnetic nanoparticles functionalized with hydrous lanthanum oxide. J Colloid Interface Sci 465:76–82. https://doi.org/10.1016/j.jcis.2015.11.043

Lee J, Walker HW (2011) Adsorption of microcystin-Lr onto iron oxide nanoparticles. Colloids Surf A Physicochem Eng Asp 373(1–3):94–100. https://doi.org/10.1016/j.colsurfa.2010.10.032

Li H, Ru JY, Yin W, Liu XH, Wang JQ (2009) Removal of phosphate from polluted water by lanthanum doped vesuvianite. J Hazard Mater 168:326–330. https://doi.org/10.1016/j.jhazmat.2009.02.025

Li D, Min H, Jiang X, Ran X, Zou L (2013) One-pot synthesis of aluminum-containing ordered mesoporous silica MCM-41 using coal fly ash for phosphate adsorption. J Colloid Interface Sci 404(32):42–48. https://doi.org/10.1016/j.jcis.2013.04.018

Likodimos V, Han C, Pelaez M, Kontos AG, Liu G, Zhu D, Liao S, de la Cruz AA, O'Shea K, Dunlop PSM, Byrne JA, Dionysiou DD, Falaras P (2013) Anion-doped TiO2 Nanocatalysts for water purification under visible light. Ind Eng Chem Res 52(39):13957–13964. https://doi.org/10.1021/ie3034575

Liu S, Li J, Yang Y, Wang J, Ding H (2016) Influence of environmental factors on the phosphorus adsorption of lanthanum-modified bentonite in eutrophic water and sediment. Environ Sci Pollut R 23:2487–2494. https://doi.org/10.1007/s11356-015-5453-z

Lu SG, Bai SQ, Zhu L, Shan HD (2009) Removal mechanism of phosphate from aqueous solution by fly ash. J Hazard Mater 161(1):95–101. https://doi.org/10.1016/j.jhazmat.2008.02.123

Lürling M, Waajen G, van Oosterhout F (2014) Humic substances interfere with phosphate removal by lanthanum modified clay in controlling eutrophication. Water Res 54:78–88. https://doi.org/10.1016/j.watres.2014.01.059

Melnyk PB (1974) Precipitation of phosphates in sewage with lanthanum: an experimental and modelling study. In: Norman JD, Doctoral dissertation, Canada Research. http://hdl.handle.net/11375/14316

Meneely JP, Elliott CT (2013) Microcystins: measuring human exposure and the impact on human health. Biomarkers 18(8):639–649. https://doi.org/10.3109/1354750X.2013.841756

Midorikawa I, Aoki H, Omori A, Shimizu T, Kawaguchi Y, Kassai K, Murakami T (2008) Recovery of high purity phosphorus from municipal wastewater secondary effluent by a high-speed adsorbent. Water Sci Technol J Int Assoc Water Pollut Res 58(8):1601–1607. https://doi.org/10.2166/wst.2008.537

Ning P, Bart HJ, Li B, Lu X, Zhang Y (2008) Phosphate removal from wastewater by model-La(III) zeolite adsorbents. J Environ Sci (China) 20(6):670–674

O'Neil JM, Davis TW, Burford MA, Gobler CJ (2012) The rise of harmful cyanobacteria blooms: the potential roles of eutrophication and climate change. Harmful Algae 14:313–334. https://doi.org/10.1016/j.hal.2011.10.027

Park JA, Jung SM, Yi IG, Choi JW, Kim SB (2017) Adsorption of microcystin-LR on mesoporous carbons and its potential use in drinking water source. Chemosphere 177:15–23. https://doi.org/10.1016/j.chemosphere.2017.02.150

Pavagadhi S, Tang ALL, Sathishkumar M, Loh KP, Balasubramanian R (2013) Removal of microcystin-LR and microcystin-RR by graphene oxide: adsorption and kinetic experiments. Water Res 47(13):4621–4629. https://doi.org/10.1016/j.watres.2013.04.033

Pelaez M, Falaras P, Likodimos V, O'Shea K, de la Cruz AA, Dunlop PSM, Byrne JA, Dionysiou DD (2016) Use of selected scavengers for the determination of NF-TiO2 reactive oxygen species during the degradation of microcystin-LR under visible light irradiation. J Mol Catal A Chem 425:183–189. https://doi.org/10.1016/j.molcata.2016.09.035

Pieterse NM, Bleuten W, Rgensen SJ (2003) Contribution of point sources and diffuse sources to nitrogen and phosphorus loads in lowland river tributaries. J Hydrol 271:213–225

Qiu H, Liang C, Yu J, Zhang Q, Song M, Chen F (2017) Preferable phosphate sequestration by nano-La(III) (hydr)oxides modified wheat straw with excellent properties in regeneration. Chem Eng J 315:345–354. https://doi.org/10.1016/j.cej.2017.01.043

Richardson SD (2007) Water analysis: emerging contaminants and current issues. Anal Chem 79(12):4295–4324. https://doi.org/10.1021/ac070719q

Rodríguez-González V, Alfaro SO, Torres-Martínez LM, Cho S, Lee S (2010) Silver–TiO2 nanocomposites: synthesis and harmful algae bloom UV-Photoelimination. Appl Catal B Environ 98(3–4):229–234. https://doi.org/10.1016/j.apcatb.2010.06.001

Saha B, Chakraborty S, Das G (2009) A mechanistic insight into enhanced and selective phosphate adsorption on a coated carboxylated surface. J Colloid Interface Sci 331:21–26. https://doi.org/10.1016/j.jcis.2008.11.007

Sathishkumar M, Pavagadhi S, Mahadevan A, Balasubramanian R, Burger DF (2010a) Removal of a potent cyanobacterial hepatotoxin by peat. J Environ Sci Health A 45(14):1877–1884. https://doi.org/10.1080/10934529.2010.520598

Sathishkumar M, Pavagadhi S, Vijayaraghavan K, Balasubramanian R, Ong SL (2010b) Experimental studies on removal of microcystin-LR by peat. J Hazard Mater 184(1–3):417–424. https://doi.org/10.1016/j.jhazmat.2010.08.051

Schroeder D (1984) Soils – facts and concepts. Internationales Kali-Institut, Bern

Şengül AB, Ersan G, Tüfekçi N (2018) Removal of intra- and extracellular microcystin by submerged ultrafiltration (UF) membrane combined with coagulation/flocculation and powdered activated carbon (PAC) adsorption. J Hazard Mater 343:29–35. https://doi.org/10.1016/j.jhazmat.2017.09.018

Su Y, Deng Y, Du Y (2013) Alternative pathways for photocatalytic degradation of microcystin-LR revealed by TiO2 nanotubes. J Mol Catal A Chem 373:18–24. https://doi.org/10.1016/j.molcata.2013.02.031

Suzuki Y, Saitoh H, Kamata Y, Aihara Y, Tateyama Y (1989) Precipitation Incidence of the Lanthanoid(III) Hydroxides: II. Precipitation from chloride and perchlorate solutions. J Less Common Met 149:179–184

Tachikawa T, Tojo S, Kawai K, Endo M, Fujitsuka M, Ohno T, Nishijima K, Miyamoto Z, Majima T (2004) Photocatalytic oxidation reactivity of holes in the sulfur- and carbon-doped TiO2 powders studied by time-resolved diffuse reflectance spectroscopy. J Phys Chem B 108(50):19299–19306. https://doi.org/10.1021/jp0470593

Teng W, Wu Z, Fan J, Chen H, Feng D, Lv Y, Wang J, Asirid AM, Zhao D (2013) Ordered mesoporous carbons and their corresponding column for highly efficient removal of microcystin-LR. Energy Environ Sci 6:2765–2776

Tian S, Jiang P, Ning P, Su Y (2009) Enhanced adsorption removal of phosphate from water by mixed lanthanum/aluminum pillared montmorillonite. Chem Eng J 151(1–3):141–148. https://doi.org/10.1016/j.cej.2009.02.006

Triantis TM, Fotiou T, Kaloudis T, Kontos AG, Falaras P, Dionysiou DD, Pelaez M, Hiskia A (2012) Photocatalytic degradation and mineralization of microcystin-LR under UV-A, solar and visible light using nanostructured nitrogen doped TiO2. J Hazard Mater 211–212:196–202

Tu C, Wang S, Qiu W, Xie R, Hu B. (2016) Phosphorus removal from aqueous solution by adsorption onto la-modified clinoptilolite. Matec Web of Conferences, 67. https://doi.org/10.1051/matecconf/2016

Urano K, Tachikawa H, Kitajima M (1992) Process development for removal and recovery of phosphorus from wastewater by a new adsorbent. 4. Recovery of phosphate and aluminum from desorbing solution. Ind Eng Chem Res 31(6):1513–1515. https://doi.org/10.1021/ie00006a013

Vimont A, Goupil J, Lavalley J, Daturi M, Surblé S, Serre C, Millange F, Férey G, Audebrand N (2006) Investigation of acid sites in a Zeotypic Giant pores chromium(III) carboxylate. J Am Chem Soc 128(10):3218–3227. https://doi.org/10.1021/ja056906s

Wang F, Gao Y, Sun Q, Chen Z, Megharaj M (2014) Degradation of microcystin-LR using functional clay supported bimetallic Fe/Pd nanoparticles based on adsorption and reduction. Sep Purif Technol 170:337–343. https://doi.org/10.1016/j.cej.2014.06.003

Wang X, Wang X, Ma R, Wang J, Tong X, Chen Y (2017) Efficient visible light-driven in situ photocatalytic destruction of harmful alga by worm-like N,P co- doped TiO2/expanded graphite carbon layer (NPT- EGC) floating composites. Cat Sci Technol 7:2335–2346

Wei G, Quan X, Fan X, Chen S, Zhang Y (2017) Carbon-nanotube-based Sandwich-like hollow Fiber membranes for expanded microcystin-LR removal applications. Chem Eng J 319:212–218. https://doi.org/10.1016/j.cej.2017.02.125

Wiegand C, Pflugmacher S (2005) Ecotoxicological effects of selected cyanobacterial secondary metabolites a short review. Toxicol Appl Pharmacol 203(3):201–218. https://doi.org/10.1016/j.taap.2004.11.002

Wolf D, Georgic W, Klaiber HA (2017) Reeling in the damages: harmful algal blooms' impact on Lake Erie's recreational fishing industry. J Environ Manag 199:148–157. https://doi.org/10.1016/j.jenvman.2017.05.031

Wu R, Lam KH, Lee J, Lau TC (2007) Removal of phosphate from water by a highly selective La(III)-chelex resin. Chemosphere 69:289–294. https://doi.org/10.1016/j.chemosphere.2007.04.022

Wu L, Lan J, Wang S, Zhu J (2017a) Synthesis of N-doped carbon Xerogel (N-CX) and its applications for adsorption removal of microcystin-LR. Z Phys Chem 231(9). https://doi.org/10.1515/zpch-2016-0912

Wu S, Lv J, Wang F, Duan N, Li Q, Wang Z (2017b) Photocatalytic degradation of microcystin-LR with a nanostructured photocatalyst based on upconversion nanoparticles@TiO2 composite under simulated solar lights. Sci Rep-UK 7(1). https://doi.org/10.1038/s41598-017-14746-6

Xia W, Zhang X, Xu L, Wang Y, Linc J, Zou R (2013) Facile and economical synthesis of metal–organic framework MIL-100(Al) gels for high efficiency removal of microcystin-LR. RSC Adv 3:11007–11013. https://doi.org/10.1039/C3RA40741A

Xie J, Lin Y, Li C, Wu D, Kong H (2015) Removal and recovery of phosphate from water by activated aluminum oxide and lanthanum oxide. Powder Technol 269:351–357. https://doi.org/10.1016/j.powtec.2014.09.024

Yan H, Gong A, He H, Zhou J, Wei Y (2006) Adsorption of microcystins by carbon nanotubes. Chemosphere 62:142–148. https://doi.org/10.1016/j.chemosphere.2005.03.075

Yang J, Zhou L, Zhao L, Zhang H, Yin J (2011) A designed nanoporous material for phosphate removal with high efficiency. J Mater Chem 21:2489–2494. https://doi.org/10.1039/c0jm02718a

Yang J, Yuan P, Chen HY, Zou J, Yuan Z (2012) Rationally designed functional macroporous materials as new adsorbents for efficient phosphorus removal. J Mater Chem A 22:9983–9990. https://doi.org/10.1039/c2jm16681j

Yang J, Zeng Q, Peng L, Lei M, Song H, Tie B, Gu J (2013) La-EDTA coated Fe3O4 nanomaterial: preparation and application in removal of phosphate from water. J Environ Sci China 25(2):413–418. https://doi.org/10.1016/S1001-0742(12)60014-X

Yang K, Yan L, Yang Y, Yu S, Shan R, Yu H, Zhu B, Du B (2014) Adsorptive removal of phosphate by Mg–Al and Zn–Al layered double hydroxides: kinetics, isotherms and mechanisms. Sep Purif Technol 124:36–42. https://doi.org/10.1016/j.seppur.2013.12.042

Yu Y, Chen JP (2015) Key factors for optimum performance in phosphate removal from contaminated water by a Fe-Mg-La tri-metal composite sorbent. J Colloid Interface Sci 445:303–311. https://doi.org/10.1016/j.jcis.2014.12.056

Yu X, Zhou J, Wang Z, Cai W (2010) Preparation of visible light-responsive AgBiO3 bactericide and its control effect on the Microcystis aeruginosa. J Photochem Photobiol B Biol 101(3):265–270. https://doi.org/10.1016/j.jphotobiol.2010.07.011

Zamparas M, Zacharias I (2014) Restoration of eutrophic freshwater by managing internal nutrient loads. A review. Sci Total Environ 496:551–562. https://doi.org/10.1016/j.scitotenv.2014.07.076

Zeng L, Li X, Liu J (2004) Adsorptive removal of phosphate from aqueous solutions using iron oxide tailings. Water Res 38(5):1318–1326. https://doi.org/10.1016/j.watres.2003.12.009

Zhang X, Jiang L (2011) Fabrication of novel rattle-type magnetic mesoporous carbon microspheres for removal of microcystins. J Mater Chem A 21:10653–10657. https://doi.org/10.1039/c1jm12263k

Zhang G, Liu H, Liu R, Qu J (2009) Removal of phosphate from water by a Fe-Mn binary oxide adsorbent. J Colloid Interface Sci 335:168–174. https://doi.org/10.1016/j.jcis.2009.03.019

Zhang J, Lei J, Xu C, Ding L, Ju H (2010) Carbon nanohorn sensitized electrochemical immunosensor for rapid detection of microcystin-LR. Anal Chem 82:1117–1122. https://doi.org/10.1021/ac902914r

Zhang G, Zhang YC, Nadagouda M, Han C, O'Shea K, El-Sheikh SM, Ismail AA, Dionysiou DD (2014) Visible light-sensitized S, N and C co-doped polymorphic TiO2 for photocatalytic destruction of microcystin-LR. Appl Catal B Environ 144:614–621. https://doi.org/10.1016/j.apcatb.2013.07.058

Zhang Y, Pan B, Shan C, Gao X (2016) Enhanced phosphate removal by Nanosized hydrated La(III) oxide confined in cross-linked polystyrene networks. Environ Sci Technol 50(3):1447–1454. https://doi.org/10.1021/acs.est.5b04630

Zhang X, Sun F, He J, Xu H, Cui F (2017) Robust phosphate capture over inorganic adsorbents derived from lanthanum metal organic frameworks. Chem Eng J 326:1086–1094. https://doi.org/10.1016/j.cej.2017.06.052

Zhou Q, Gibson CE, Zhu Y (2001) Evaluation of phosphorus bioavailability in sediments of three contrasting lakes in China and the UK. Chemosphere 42:221–225. https://doi.org/10.1016/S0045-6535(00)00129-6

Zong E, Liu X, Wang J, Yang S, Jiang J, Fu S (2017) Facile preparation and characterization of lanthanum-loaded carboxylated multi-walled carbon nanotubes and their application for the adsorption of phosphate ions. J Mater Sci 52(12):7294–7310. https://doi.org/10.1007/s10853-017-0966-0